Materials and Structures (2021)xx:xx
https://doi.org/10.1617/s11527-021-01624-x

ORIGINAL ARTICLE

Experimental and theoretical study of bond behaviour between FRP bar and high-volume fly ash-self-compacting concrete

Yu Zheng · Nuan Zhou · Lingzhu Zhou · Hexin Zhang · Haotian Li · Yingwu Zhou

Received: 27 September 2020 / Accepted: 5 January 2021

Abstract The combination of fibre-reinforced polymer (FRP) and high-volume fly ash self-compacting concrete (HVFA-SCC) reinforced is expected to solve the problem of steel corrosion in traditional structures and develop sustainable infrastructures. Bond behaviour has a strong effect on serviceability of FRP reinforced concrete structures. To achieve the acceptance of this novel composite structures in practical construction and design, it is significantly important to investigate the bond behaviour of FRP reinforced HVFA-SCC. In this study, a series of pull-out tests were carried out to investigate the bond behaviour of HVFA-SCC reinforced by FRP bar, which included bond strength, bond-slip response, and failure mode. The investigated experimental variables were reinforcing materials, surface treatment of FRP bars, bar diameters and concrete materials. The test results revealed that using HVFA-SCC resulted in higher average bond strength compared to those in the normal concrete test specimens. The reinforcing materials (steel vs. GFRP) had strong effect on bond behaviour, including bond strength, bond stiffness and failure mode. The failure mechanism of bond interaction between FRP and HVFA-SCC is dependent on friction and chemical adhesion. Subsequently, theoretical models for bond strength and development length were proposed. Finally, the parameters of analytical models of bond-slip curve are calibrated for GFRP reinforced HVFA-SCC by using the experimental data.

Y. Zheng (✉) · L. Zhou · H. Li
School of Environment and Civil Engineering, Dongguan University of Technology, Dongguan 523080, China
e-mail: zhengy@dgut.edu.cn

L. Zhou
e-mail: lingzhu_zhou@163.com

H. Li
e-mail: 495443523@qq.com

N. Zhou
School of Mechanics and Civil Engineering, China University of Mining and Technology-Beijing, Beijing 100083, China
e-mail: 1357342044@qq.com

L. Zhou
Key Laboratory of Coastal and Offshore Engineering, Dalian University of Technology, Dalian 116024, China

H. Zhang
School of Engineering and the Built Environment, Edinburgh Napier University, Edinburgh, UK
e-mail: j.zhang@napier.ac.uk

H. Li · Y. Zhou
College of Civil and Transportation Engineering, Shenzhen University, Shenzhen, China
e-mail: ywzhou@szu.edu.cn

Keywords Fibre reinforced polymer (FRP) bars · High-volume fly ash self-compacting concrete (HVFA-SCC) · Bond-slip behaviour · Bond failure mechanism · Analytical models

1 Introduction

The service life of steel reinforced concrete structures is reduced by the corrosion of steel bars, especially in marine or near aggressive environments [1]. In addition, a large amount of energy is consumed induced by the cement production. In fact, 5–7% of global carbon dioxide emissions comes from cement production [2]. Therefore, structural performance degradation of concrete infrastructure and the development of high-performance concrete materials with low carbon footprint are the major challenges. Many engineers and researchers have proposed some viable alternative construction materials. For the steel-corrosion problems, fibre reinforced polymer (FRP) can be used as internal reinforcing materials instead of steel reinforcement, which can also improves the durability of those structures [3]. Additionally, by using post-waste materials, such as fly ash, ground, limestone powder and granulated blast furnace slag, self-compacting concrete (SCC) has the characteristics of high-performance, low-energy consumption, high flowability and convenient construction [4, 5]. It has been reported that the SCC mixed with high-volume fly ash (50% or more) can produce an environmentally friendly concrete with high flowability and durability [6]. Therefore, these two engineering materials, high-volume fly ash-SCC (HVFA-SCC) and FRP, have attracted wide attention in the structural constructions [7]. Due to those advantages of FRP reinforcement and HVFA-SCC, combining the two materials can offer a promising technology to solve two sustainability problems (steel corrosion and high carbon footprint) [8]. FRP reinforced concrete structures have larger deflection and crack width than steel reinforced concrete structures [8, 9]. The service behaviour, including deflection and crack width, is affected by the bond behaviour of FRP and concrete. Also, the research on the structural behaviour of HVFA-SCC reinforced by FRP bars is rather limited. To achieve widespread acceptance of the combination of the two materials in practical constructions, it is necessary to investigate the bond behaviour between FRP and HVFA-SCC for ensuring a good load-transferring mechanism.

The bond behaviour of FRP reinforced concrete is inferior to that of steel reinforced concrete structures [10–12]. This is attributed to different surface treatments and the low axial stiffness of FRP bars. The influence of the embedment length, rebar type and rebar diameter on the bond behaviour of FRP reinforced normal concrete (NC) has been studied widely [13]. The compositions of HVFA-SCC are different from that of NC, which could result in the various internal microstructure and mechanical properties between FRP reinforced HVFA-SCC specimen and FRP reinforced NC specimen [14, 15]. It has been reported that the concrete compositions, including powder types and content, aggregate types and contents, and admixture, have a significant effect on the bond properties [16, 17]. This means that the FRP/steel reinforced HVFA-SCC, SCC and NC have different bond behaviour. Existing studies shows that using SCC to replace normal concrete (NC) can result in higher or equal bond behaviour, which is due to its higher compactness and filling properties [18]. In addition, the lower variability of bond stress is presented in SCC rather than NC [19]. Arezoumandi et al. [20] found that the similar bond strength is presented in the steel reinforced HVFA-SCC and the steel reinforced NC. Martí-Vargas et al. [21] indicated that the transmission length is affected by the compositions of concrete. Currently, bond behaviour of GFRP reinforced HVFA-SCC is rarely discussed in the existing literature. Therefore, it is of significantly important to fully study the bond-slip behaviour and bond failure process between GFRP bars and HVFA-SCC for establishing the prediction model of bond strength and development length. This is beneficial for developing further study on the serviceability behaviour and establishing the design guidelines of FRP reinforced HVFA-SCC structures.

In this paper, a series of direct pull-out tests were conducted to investigate the bond-slip behaviour of FRP and HVFA-SCC. The structural variables adopted in this study include reinforcing materials, geometry and surface treatments of GFRP bars, GFRP bar diameters and concrete materials. Also, the test results are used to discuss the influence of those parameters on the bond strength, failure mechanism and bond-slip relationship of FRP reinforced HVFA-

SCC specimens. The results of interface damage can be verified by the test results of piezoelectric ceramic sensors given in Reference [22]. Considering the influence of filling performance of HVFA-SCC on bond properties, the theoretical models of bond strength and development length of GFRP reinforced HVFA-SCC are proposed. Finally, the parameters of analytical models of FRP reinforced HVFA-SCC bond slip curves are calibrated by using test data. The Ttst results indicate that the average bond strength of GFRP reinforced HVFA-SCC specimens is higher than that of GFRP reinforced NC specimens, especially in specimen of GFRP with a lower spiral height.

2 Experimental program

The properties of the adopted raw materials and the test procedures conducted to investigate the bond-slip behaviour of FRP reinforced HVFA-SCC are discussed in this section.

2.1 Materials

Three reinforcing bars (GFRP, BFRP and steel) provided by three manufacturer companies were used in this test. The surface treatments of these bars are presented in Fig. 1. The GFPR and BFRP bars had spiral wound surfaces. In addition, the surface of the GFRP bars is coated with silica sand, which helps improve the bond behaviour by enhancing friction and interlock forces [23]. To study the effects of spiral height on bond behaviour, two types of GFRP bars with different spiral heights were adopted in this test. Additionally, the ribbed steel bars were employed for comparison purposes. The test results of the mechanical properties of reinforcing bars are shown in Table 1.

The binder materials for the preparation of HVFA-SCC were composite Portland cement, fly ash and limestone powder. Crushed granite with a particle size of 4.75–16 mm as coarse aggregate and river sand with a fineness modulus of 2.39 as fine aggregate were used in this test, respectively. BASF-F10 superplasticizer was used to improve the fluidity of HVFA-SCC. The compositions of HVFA-SCC and NC are summarized in Table 2. In the production of the HVFA-SCC mixtures, controlling the mixing sequence and time is essential for the workability of HVFA-SCC.

Fig. 1 Surface treatments of reinforcing bars

The one-time mixing method was adopted to produce HVFA-SCC. The batching sequence consisted of homogenising all the mixture except water for 120 s in a single horizontal-axis forced mixer. Then, 50% of the water was added into the mixer and continue to mix for 60 s at the same speed. Finally, the remaining water was added and the concrete was mixed for a further 120 s. The slump flow diameter (the slump for NC), the J-ring diameter, the U-Box height difference and the V-funnel time were tested to determine the workability of fresh HVFA-SCC. The test procedure is shown in Fig. 2 and the test results are listed in Table 3.

In this test, three cubes (150 × 150 × 150 mm) and three cylinders (300 × 150 mm) were respectively poured for both HVFA-SCC and NC to determine its compressive strength and elasticity modulus. The test specimens were demoulded after 24 h of concrete pouring and then were cured for another 55 days under the condition of 20 ± 2 °C and 95% humidity. The mechanical properties of hardened concrete are listed in Table 3.

2.2 Preparation of pull-out test specimens

One end of the FRP bar is enclosed by a steel tube and the inside is filled with epoxy adhesive, which aims to prevent FRP bas from failing due the gripping forces applied by the clamps of the hydraulic machine during

Table 1 Geometric and mechanical properties of reinforcing bars

Rebar type	Diameter (mm)	Surface treatment[a]	Spiral height (mm)	Spiral spacing (mm)	Ultimate strength (MPa)	Elastic modulus (GPa)	Strain at ultimate strength (%)
GFRP	13	SWSC	0.21	22.9	1126	54	2.0
GFRP	13	SWSC	0.51	24.3	1003	52	1.9
GFRP	19	SWSC	0.30	19.5	882	48	1.8
BFRP	12	SWS	0.45	11.9	1053	50	2.1
Steel	13	SR	0.89	7.5	589	210	10.0

[a]*SWSC* spiral wound and sand coated, *SWS* spiral wound surface, *SR* steel ribs

Table 2 Compositions of HVFA-SCC and NC

Concrete type[a]	Fly ash (kg)	Cement (kg)	Limestone powder (kg)	River sand (kg)	Granite (kg)	Water (kg)	Superplasticizer (kg)
HVFA-SCC-50%	22.19	16.64	5.55	67.73	49.05	13.76	0.089
HVFA-SCC-65%	28.84	9.98	5.55	67.73	49.05	13.76	0.089
NC	–	44.72	–	34.66	77.15	18.47	–

[a]HVFA-SCC-50% means that fly ash accounts for 50% of cementitious material; HVFA-SCC-65% means that fly ash accounts for 65% of cementitious material; *NC* normal concrete

Fig. 2 The test procedure of the workability of HVFA-SCC

Table 3 The results of fresh and hardened properties of HVFA-SCC and NC

Concrete types	Slump flow[a] diameter (mm)	Slump (mm)	J-ring diameter (mm)	U-Box difference (mm)	V-funnel time (s)	Compressive strength (MPa)	Tensile strength (MPa)	Elastic modulus (GPa)
SCC-50%	692	–	682	21	9.1	45.4	3.8	32.5
SCC-65%	765	–	761	4	6.8	21.5	1.8	21.5
NC	–	74	–	–	–	52.1	4.4	36.9

[a]For NC, the slump test was carried out

testing. After curing the epoxy, the FRP and steel bars were embedded in the centre of the concrete sample, which had dimensions of 200 × 200 × 200 mm. The bond lengths were determined using five times of the diameters of the reinforcing bars ($l = 5d$) and can be achieved by using two PVC pipes in the unbonded areas of the reinforcing bars. To control the expansion of wood moulds in concrete casting, metal moulds were used for all the test specimens. All the test specimens were removed from the steel moulds a week after casting.

2.3 Test setup

The test method for a direct pull-out test reported in ACI 440.3 R-12 standard [24] was adopted in this test to investigate the bond behaviour of FRP reinforced HVFA-SCC. The pull-out loading test setup and data acquisition system are presented in Fig. 3. The pull-out tests were carried out by using a microcomputer-controlled electro-hydraulic servo universal testing machine with a capacity of 1000 kN. The displacement loading control at a rate of 0.02 mm/s was adopted in all direct pull-out test specimens, which aims to capture the post-failure behaviour in the bond-slip relationships. As shown in Fig. 3a, four linear variable differential transformers (LVDTs) were symmetrically placed at the loaded and unloaded end of the test specimens for measuring the slip values during the loading test. Those LVDTs were connected to TDS-530 data acquisition instrument for obtaining these slip values of loaded and unloaded end. The applied load was recorded by the computer connected to test machine. During loading, these slip values and applied load were continuously collected synchronously at a rate of one acquisition per second. It is worth noting that the slip values at the loading end are not discussed in the following section and the slip values of unloaded end were used as the overall slips. In addition, the configuration for the piezoelectric test is shown in Fig. 3c. The piezoelectric signals were recorded synchronously in the pull-out test and the piezoelectric test results had been discussed in detail in Reference [22]. In this paper, the piezoelectric test results are used to verify the results of interface damage. In this test, a total of 24 test specimens were tested up to failure.

3 Test result and discussion

In this test, the influence of concrete materials, reinforcing materials, FRP bar surface treatment and FRP bar diameter is discussed. In the pull-out test, it is assumed that the bond stress of reinforcing bars and concrete is evenly distributed along the bond length. The average bond stress, τ, is defined as:

$$\tau = P/\pi dl \quad (1)$$

where P is the ultimate tensile load, d is the bar diameter and l is the bond length. The relationship between the average bond stress determined by Eq. (1)

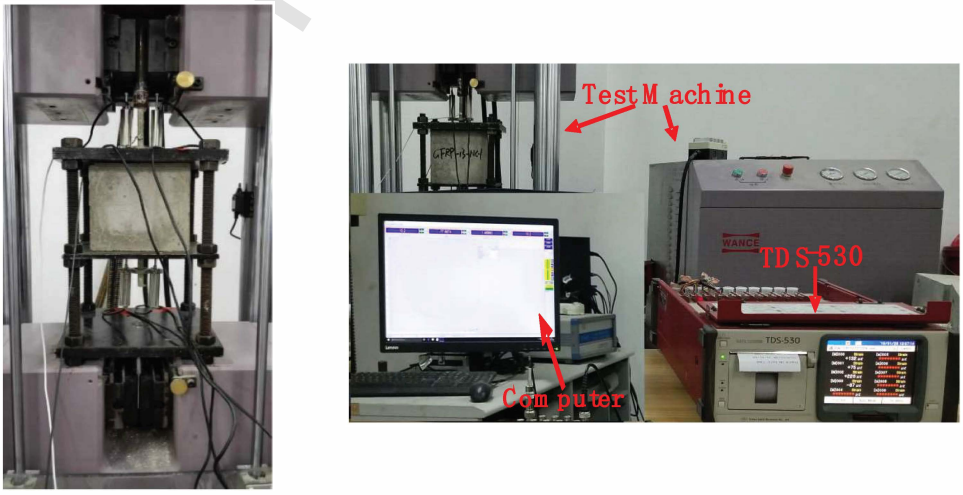

(a) Pullout loading test setup **(b) Data acquisition system**

Fig. 3 Bond test configuration

Table 4 Experimental results for all specimens

Specimen [a]	P_{max} (kN)	τ_{max} (MPa)	τ_{max} [b] (MPa)	S_u [c] (mm)	S_u [d] (mm)	Failure mode
G-13-50%-45.4-1	28.69	10.81	10.96	0.21	0.25	Pull out
G-13-50%-45.4-2	29.46	11.10		0.28		Pull out
G-13-50%-45.4-3	–	–	–	–	-	Pull out
G-13-50%-45.4-1*	34.77	13.10	11.79	7.42	7.84	Pull out
G-13-50%-45.4-2*	28.92	10.89		9.04		Pull out
G-13-50%-45.4-3*	30.24	11.39		7.05		Pull out
G-19-50%-45.4-1	15.34	2.71	3.56	4.62	4.66	Pull out
G-19-50%-45.4-2	25.19	4.44		5.81		Pull out
G-19-50%-45.4-3	20.03	3.53		3.55		Pull out
G-13-NC-52.1-1	22.06	6.99	6.18	0.05	0.08	Pull out
G-13-NC-52.1-2	16.27	5.13		0.12		Pull out
G-13-NC-52.1-3	17.04	6.42		0.07		Pull out
G-13-NC-52.1-1*	24.38	10.78	10.28	6.54	7.83	Pull out
G-13-NC-52.1-2*	23.05	10.19		8.44		Pull out
G-13-NC-52.1-3*	22.31	9.87		8.52		Pull out
G-13-65%-21.5-1	27.85	10.49	10.69	0.17	0.20	Pull out
G-13-65%-21.5-2	28.68	10.80		0.19		Pull out
G-13-65%-21.5-3	28.62	10.78		0.24		Pull out
B-12-50%-45.4-1	31.93	13.03	11.75	2.58	2.58	Pull out
B-12-50%-45.4-2	26.73	10.91		2.13		Pull out
B-12-50%-45.4-3	27.72	11.31		3.02		Pull out
S-13-50%-45.4-1	51.03	19.22	20.39	0.90	0.76	Pull out
S-13-50%-45.4-2	57.27	21.57		0.69		Pull out
S-13-50%-45.4-3	54.10	20.38		0.70		Pull out

[a]*Represents 13 mm GFRP bars with a spiral height of 0.51 mm

[b]Average value of bond strength of specimens in the same working condition

[c]Unloaded end slip when bond strength is reached

[d]Average value of corresponding slip of specimens in the same working condition

and the unloaded end slip value is used to analyse the bond properties. The pull-out specimen identification is as follows:

- The first letter indicates the bar type (G for GFRP bar, B for BFRP bar and S for steel bar);
- The first number indicates the rebar diameter in mm;
- The second letter denotes the type of concrete (NC and HVAF-SCC);
- The second number indicates the concrete compressive strength in MPa;
- The last number indicates specimen number.

For example, the G-13-SCC-45.4-1 designates the first specimen of the GFRP bar with the 13 mm diameter reinforced SCC with a compressive strength of 45.4 MPa.

The experimental results obtained from the pull-out tests are listed in Table 4. It is worth mentioning that the failure mode of pull-out was found in all test specimens since sufficient transverse restraint was provided by the relatively thick concrete cover.

3.1 Bond strength

The failure load and bond strength of all the test specimens are summarised in Table 4. The recorded

average bond strength for the test specimens of steel reinforced HVFA-SCC (S-13-50%-series) is about two times higher than that of FRP reinforced HVFA-SCC test specimens (G-13-50%-series and B-12-50%-series). This contributed to the higher axial stiffness of steel reinforcement compared to FRP bars and steel-ribbed surface treatment. It could introduce different failure modes in the steel and FRP reinforced HVFA-SCC specimens, which will be discussed in the next section. Fly ash and limestone powder, as the substitutes for cement cementitious material, were added into HVFA-SCC, which can improve the compactness property of HVFA-SCC [25, 26]. As a result, using HVFA-SCC to replace NC resulted in higher bond strength in this test due to the denser internal structure and stronger chemical adhesion. Interestingly, spiral height has a slight effect on the bond strength of the test specimens of HVFA-SCC, while bond strength of the test specimens of NC is increased by about 80% when the spiral height of GFRP bars increases from 0.21 to 0.51 mm. This mean that the contribution of spiral height to bond strength is reduced in HVFA-SCC due to its high interfacial compactness. In addition, increasing fly ash volume in HVFA-SCC has barely effect on the peak bond strength. As reported in the literature [27–29], increasing the diameter of the GFRP bars results in a decrease in the average bond strength. This phenomenon can be explained for by the following reasons: (a) An uneven distribution of normal stresses through the cross section of the bar is presented in the pull-out of FRP bar, which results in a lower average bond strength; (b) Longer embedment length is required to develop the same normal bond stress for larger diameter bars, and the nonlinear stress distribution along the direction of the embedment length reduces the average bond strength; (c) The contact interface between concrete and FRP bar is increased by increasing the diameter of the reinforcing bar, and a large amount of water in concrete is absorbed and retained at the interface, reducing the chemical adhesion and frictional stresses. Thus, the average bond strength is decreased by increasing the diameter of the GFRP bars.

3.2 Failure mechanism

The common failure mode observed in all the test specimens is the pull-out failure of GFRP bars in HVFA-SCC. This is due to the fact that the short development length for the bonding test cannot result in wider longitudinal cracks along the concrete prism. Also, the test specimens were split to observe the interface damage and analyse the failure mechanisms of FRP reinforced HVFA-SCC, as shown in Fig. 4.

It should be noted that the reinforcing materials had a strong effect on the failure modes of the bond test specimens, as shown in Fig. 4a–c. Although the bond strength of HVFA-SCC specimens reinforced with GFRP and BFRP is similar, the surface abrasion damage of BFRP bars is more significant than GFRP bars (see Fig. 4a, b). This occurred due to the surface treatment of the BFRP bar which is formed by winding a spiral basalt fibre bundle. On account of the low elasticity modulus and weak lateral shear resistance of the fibre bundles, they were abrasion by concrete during the pull-out test. Additionally, using the sand-coated surface in the GFRP bars resulted in delamination of the resin-rich outer layer from the fibre core and damage to the concrete attached to the bar surface, as shown in Fig. 4a. These test results indicate that debonding failure of the GFRP and BFRP reinforced test specimens is dependent on friction and chemical adhesion. On the contrary, it can be found from Fig. 4c that the surface of steel bars is almost intact and some concrete blocks are inserted between the steel ribs. This means that the concrete is tore between two adjacent steel ribs in the steel reinforced HVFA-SCC specimens due to the low rib spacing-to-height ratios and enough concrete cover surrounding the steel rebar. Similar phenomena have also been observed in the references [30, 31]. It can be summarised that the steel reinforced HVFA-SCC specimens failed in the mechanical interlocking between the ribs and concrete paste and the bond strength is determined by shear strength of the surrounding concrete.

The effect of the surface geometry of GFRP bars on the bond performance has been introduced in Gu's study [32]. As the standards and quality of FRP bars produced by different manufacturers are not uniform, the surface treatment of various FRP bars is still not accurately quantified. This could make the specification of FRP bars difficult and hinder the practical application of FRP bars in new structures. The failure mode shown in Fig. 4a, d reveals that the surface damage of the GFRP bar with a spiral height of 0.51 mm is more obvious. This also indicates that increasing the spiral height of GFRP bars results in

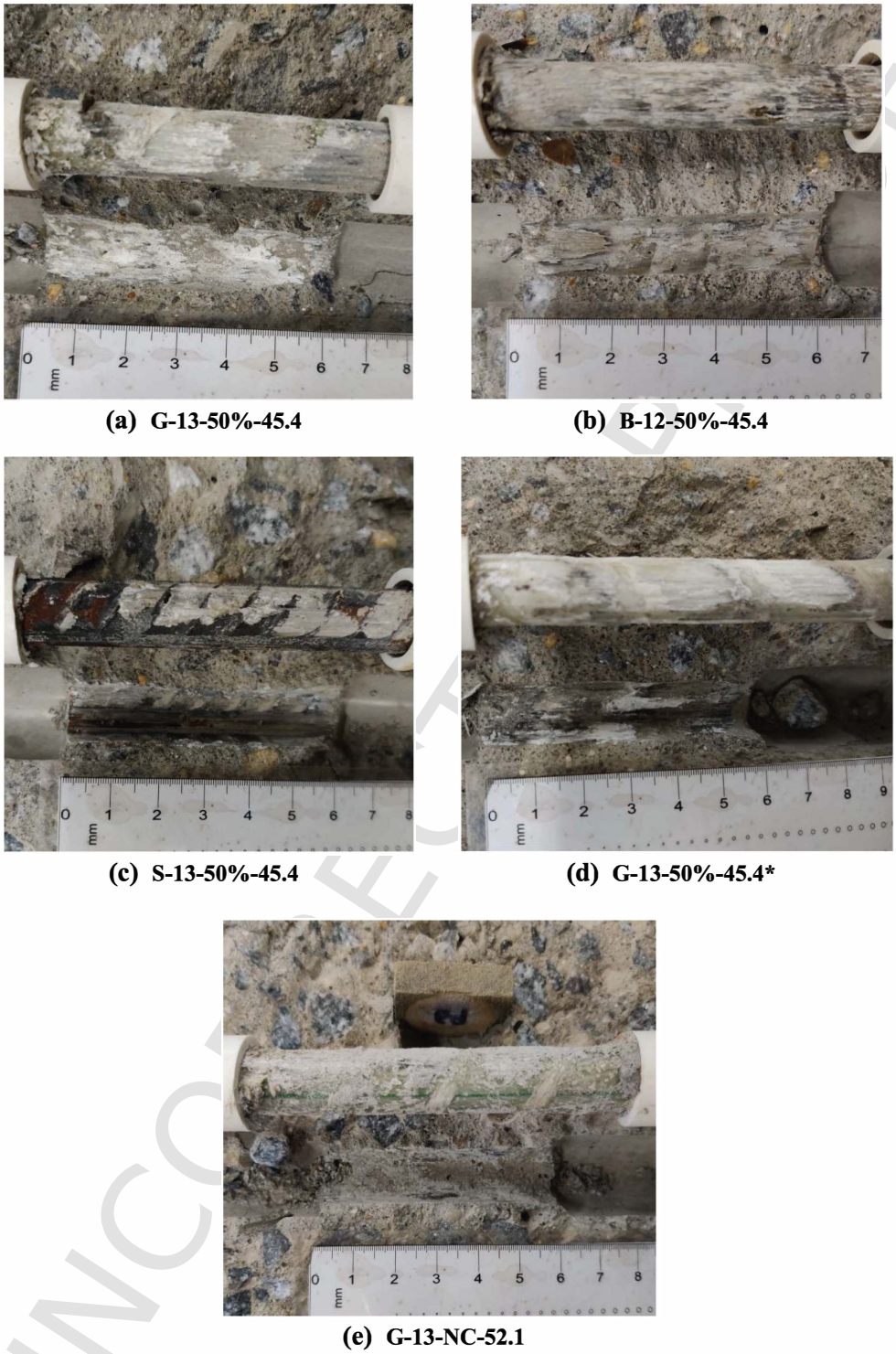

(a) G-13-50%-45.4 (b) B-12-50%-45.4

(c) S-13-50%-45.4 (d) G-13-50%-45.4*

(e) G-13-NC-52.1

Fig. 4 Interface damage of test specimens

stronger mechanical interaction between reinforcing bars and HVFA-SCC.

The influence of varying the surrounding concrete matrix materials (HVFA-SCC vs. NC) on failure mechanism in bond tests is shown in Fig. 4a, e. The surface of GFRP reinforcing bar is damaged by the delamination of the resin-rich outer in the pull-out test for the HVFA-SCC test specimens, while the surface of the GFRP bar in NC test specimens is almost intact and some residual concrete is attached to the

reinforcement. This is due to the fact that the compactness of HVFA-SCC is better than the NC due to the filling effect of fly ash and limestone powder in HVFA-SCC mixture [26, 33]. It can be inferred from the interface damage of reinforcement that the stronger adhesive and friction are presented in GFRP reinforced HVFA-SCC specimens rather than NC specimens. This results in the improvement of bond strength of GFRP reinforced HVFA-SCC specimens, which can be proved by the test result in Table 4.

As reported in the literature [22], an active sensing technology using a pair of Smart Aggregates (SA) is adopted to identify the failure mechanism of steel/FRP reinforced concrete in pull-out process. It is found that the failure of steel reinforced HVFA-SCC specimen depends on the mechanical interlocking damage, and the failure of FRP reinforced HVFA-SCC is mainly the chemical adhesion and friction damage. This is consistent with the interface damage presented in Fig. 4a–c.

3.3 Bond-slip relationship

The bond-slip behaviours of the HVFA-SCC test specimens reinforced with different bars are shown in Fig. 5a. It can be seen that the stiffness of bond-slip behaviour in steel reinforced HVFA-SCC test specimens is higher than that in GFRP and BFRP reinforced HVFA-SCC test specimens. This is owing to the high elastic modulus of steel bar and the high mechanical interlock resistance between steel bar and concrete. The similar bond behaviour is presented in GFRP and BFRP reinforced HVFA-SCC test specimens, which corresponds to the similar stiffness of the two reinforcing materials. It can be found that the slip value of the test specimens reinforced with GFRP is smaller than that of BFRP reinforced specimens. This phenomenon is due to the various surface treatments of the FRP bars. As shown Fig. 1, the surface of the GFRP bar is spiral wound with a sand coating, and the BFRP bar has a spiral wound and a large spiral spacing. In addition, the bond-slip curve of the BFRP reinforced test specimen has obvious periodic fluctuation, which is consistent with the spiral spacing of the BFRP bar. When the slip value is equal to the spiral spacing of the BFRP bar, a new "spiral wound" enters the bond length and re-provides the mechanical interaction and friction in the pull-out test. A similar periodic fluctuation behaviour has also been reported

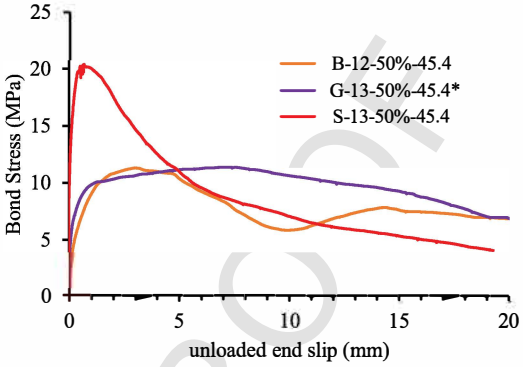

(a) The effect of the type of reinforcement bars on the bond-slip curve

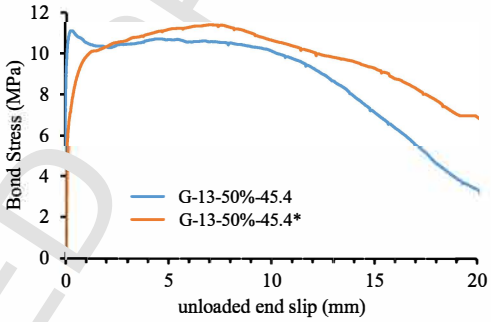

(b) The effect of the spiral height on the bond-slip curve

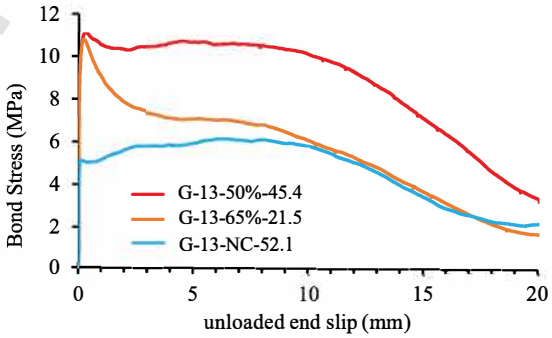

(c) The effect of the type of concrete material on the bond-slip curve

Fig. 5 Bond-slip curves of the test specimens

in CEB-FIP Model Code 90 [34] and Baena's study [27]. The spiral spacing of the GFRP bar is larger than the measuring range of the pull-out test, therefore similar periodic fluctuation behaviour cannot be exhibited in the bond-slip curve. For the purpose of comparison, the pull-out test of steel bars is also presented. Figure 5a shows that the corresponding slip value is relatively small when the bond strength is reached. The ribs on the surface of the steel bars provide a reliable mechanical interaction between steel bars and the HVFA-SCC, so that the high initial stiffness is presented in bond-slip curve. A fast bond degradation behaviour is exhibited in the descending branch of the steel bar reinforced test specimen, which

is caused by the shear damage of the concrete between the ribs during the pull-out process.

The influence of spiral height of GFRP bars on bond performance is shown in Fig. 5b. In this study, GFRP bars of the same diameter (13 mm) were used to study the effect of the surface treatments of reinforcing bars on the bond performance. It was found that the bond strength of the two spiral heights is similar but the spiral height has a significant influence on the unloaded end slip value when the bond strength is reached. The specimen reinforced by GFRP bar with large spiral leads to the increase of pores at the interface, which means that the chemical bond and friction effect are decreased at the interface of FRP bars and concrete. In the early stages of the pull-out process, the chemical bond force is the key factor to resist pull-out. Therefore, the large unloaded end slip is presented in the specimen reinforced by GFRP bar with higher spiral. The specimen using GFRP bar with larger spiral height can provide higher mechanical interaction during the pull-out process. However, the chemical bond and friction play an important role to resist pull-out force when using GFRP bars with smaller spiral height, which is due to the denser interface of FRP bars and concrete. Therefore, the lower spiral height of the GFRP bar in specimen leads to a small unloaded end slip value.

Figure 5c shows the effect of different concrete materials on the bond-slip behaviours. The variation of concrete materials does not have a significant effect on the unloaded end slip corresponding to bond failure. However, the effect of different concrete materials on the bonding degradation process is significant. The post-peak bond stress of the NC and SCC-50% series is maintained at a high level, but the post-peak bond stress of the HVFA-SCC-65% series decreases rapidly. The mechanical interlocking is negligible due to the small spiral height (0.21 mm) of GFRP bars, and the chemical adhesion is failed after the bond strength is reached. This implies that the bond stress after bond strength mainly depends on the friction between concrete and FRP reinforcement. Therefore, the compressive strengths of the concrete materials (52.1 MPa for NC, 45.4 MPa for HVFA-SCC-50%, 21.5 MPa for HVFA-SCC-65%) and the interface porosity caused by different concrete compositions are the key factors of affecting the degradation of bond slip curve after post-peak bond stress [16]. As shown in Fig. 5c, larger post-peak bond stress can be provided by the concrete with higher compressive strength, which indicates that the high compressive strength could result in the slow degradation of bond behaviour.

4 Analytical study of bond behaviour

4.1 Prediction models for bond strength and development length

The stress transfer and collaborative deformation of FRP reinforced concrete structures depend on the bond stress. The bond strength is a key factor affecting the cracking behaviour, tension stiffening, plastic hinge rotation capacity and failure mechanism of concrete members reinforced with FRP bars. Also, it is responsible for the ultimate strength of the end anchorage joint components. To determine the appropriate development length to ensure the safety of FRP reinforced concrete structures, it is important to accurately predict bond strength by using an appropriate model.

Table 5 summarises some of the models to evaluate the bond strength of FRP bars and ordinary concrete, which mainly consider factors such as compressive strength of the concrete, thickness of the concrete protective layer, diameter of the reinforcing bar and bond length, etc. The predicted values of bond strength are calculated and compared with the test results obtained from the pull-out test, and the comparison results are listed in Table 6. The bond strength of the test specimens GFRP with a diameter of 19 mm reinforced SCC and GFRP with a spiral height of 0.21 mm reinforced NC is significantly overestimated by all formulas in Table 5. This suggests that the effect of the diameter of the FRP bar on bond strength has not been accurately reflected in these models. Also, the effect of spiral height of FRP bars on the bond strength of FRP reinforced NC should be considered. For the other specimens, the bond strength is overestimated by Eqs. (5) and (6), and underestimated by Eqs. (3), (7) and (8). The calculated results of Eqs. (2) and (4) mostly overestimate bond strength except test specimens of G-13-65%-21.5. This means that the effect of compressive strength on bond strength of FRP reinforced HVFA-SCC is magnified in these formulas. Therefore, it is particularly important to put forward the prediction formula of bond strength for FRP

Table 5 The methods for calculating bond strength of FRP reinforced ordinary concrete

Prediction method	Prediction models	Equation
ACI 440.1R-06 [35]	$\tau_{max} = 0.083\sqrt{f_c}\left(4.0 + 0.3\frac{c}{d} + 100\frac{d}{l}\right)$	(2)
ACI 440.1R-03 [36]	$\tau_{max} = 20.23\frac{\sqrt{f_c}}{d}$	(3)
CEB-FIP [37]	$\tau_{max} = 13.5\left(\frac{f_c}{30}\right)^{\beta}$	(4)
Choi et al. [38]	$\tau_{max} = \sqrt{f_c}\left(0.037 + 0.151\frac{c}{d} + 7.719\frac{d}{l}\right)$	(5)
He and Tian [39]	$\tau_{max} = 4.2 + 72\left(\frac{d}{l}\right)^{1.3}$	(6)
Lee et al. [40]	$\tau_{max} = 3.3(f_c)^{0.3}$	(7)
Okelo and Yuan [12]	$\tau_{max} = 14.7\frac{\sqrt{f_c}}{d}$	(8)

τ_{max}—bond strength; f_c—axial compressive strength of concrete; c—thickness of the concrete protective layer; d—diameter of reinforcing bar; l—bond length; β—bonding coefficient

reinforced HVFA-SCC due to the variance in damage mechanism between FRP bars reinforced HVFA-SCC and reinforced NC in the process of pulling-out.

As previously reported in the literature [41] that the SCC can significantly improve the bond strength of FRP reinforced SCC members due to high cementitious materials and high density. Mousavi et al. [41] proposed a prediction formula, as shown in Eq. (9), for bond strength of GFRP reinforced SCC, which considered the ratio of fine to all amount of aggregate (*Fine/All*) to reflect the filling ability.

$$\tau_{max} = \sqrt{f_c}\left(-14.416 + 0.3716\frac{c}{d} + 3.1725\frac{d}{l} + 24.3766\frac{\text{Fine}}{\text{All}}\text{Aggregate}\right) \quad (9)$$

The calculated results of bond strength from formula (9) are given in Table 7. It can be observed that the bond strength calculated by Eq. (9) significantly overestimated the test values since a high sand-to-aggregate ratio was used to prepare HVFA-SCC in this test. Besides, the authors think that the ratio of fine-to-total aggregate cannot effectively reflect the filling ability and compactness of interface. However, the slump-flow can quantify the filling ability, and it is an important factor affecting the interfacial bonding of FRP bars and HVFA-SCC. Therefore, a new prediction formula of FRP reinforced HVFA-SCC considering the slump-flow is proposed for the pull-out test specimens with an embedment length of 5 times diameters of FRP bars in this paper, as shown below:

$$\tau_{max} = \sqrt{f_c}\left(\alpha + \beta\frac{c}{d} + \gamma SF\right) \quad (10)$$

where the coefficients α, β and γ can be obtained based on curve-fitting the test values, and the SF represents the slump-flow in mm. Based on the least square method, the coefficients can be determined and the proposed prediction formula of FRP reinforced HVFA-SCC can be expressed as follows:

$$\tau_{max} = \sqrt{f_c}\left(-9.3508 + 0.4778\frac{c}{d} + 0.0108 \times SF\right) \quad (11)$$

The results of the bond strength from the test values and from Eq. (11) are presented in Table 7. It shows that the bond strength values predicted by Eq. (11) are consistent with the test values and the average value of the COV is 0.99. This implies that the proposed predicted model for bond strength of FRP reinforced HVFA-SCC is accurate and applicable.

The development length is required in actual engineering structures to prevent the reinforcing bar from being pulled out. And the minimum development length (l_{ab}) in the pull-out test indicates that the fracture failure of the reinforcing bar and the pulled-out failure occurs simultaneously. As a result, the equilibrium equation can be established as follows:

$$\tau_{max}\pi d l_{ab} = f_{max}A_r \quad (12)$$

where the f_{max} and A represent the tensile strength and the cross section area of FRP bar, respectively. The minimum development length can be derived from Eq. (12), as shown below:

Table 6 The comparison of the test values and predicted values of bond strength, using the formulas of FRP reinforced ordinary concrete (Eqs. 2–8)

Specimen[a]	TV (MPa)	(2)		(3)		(4)		(5)		(6)		(7)		(8)	
		PV (MPa)	COV	PV (MPa)	COV	PV (MPa)	COV	PV (MPa)	COV	PV (MPa)	COV	PV (MPa)	COV	PV (MPa)	COV
G-13-50%-45.4-1	10.81	13.16	0.82	9.38	1.15	14.85	0.73	16.53	0.65	13.09	0.83	9.70	1.11	6.81	1.59
G-13-50%-45.4-2	11.10	13.16	0.84	9.38	1.18	14.85	0.75	16.53	0.67	13.09	0.85	9.70	1.14	6.81	1.63
G-13-50%-45.4-1*	13.10	13.16	1.00	9.38	1.40	14.85	0.88	16.53	0.79	13.09	1.00	9.70	1.35	6.81	1.92
G-13-50%-45.4-2*	10.89	13.16	0.83	9.38	1.16	14.85	0.73	16.53	0.66	13.09	0.83	9.70	1.12	6.81	1.60
G-13-50%-45.4-3*	11.39	13.16	0.87	9.38	1.21	14.85	0.77	16.53	0.69	13.09	0.87	9.70	1.17	6.81	1.67
G-19-50%-45.4-1	2.71	12.79	0.21	6.42	0.42	14.85	0.18	14.32	0.19	13.09	0.21	9.70	0.28	4.66	0.58
G-19-50%-45.4-2	4.44	12.79	0.35	6.42	0.69	14.85	0.30	14.32	0.31	13.09	0.34	9.70	0.46	4.66	0.95
G-19-50%-45.4-3	3.53	12.79	0.28	6.42	0.55	14.85	0.24	14.32	0.25	13.09	0.27	9.70	0.36	4.66	0.76
G-13-NC-52.1-1	6.99	14.10	0.50	10.05	0.70	15.91	0.44	17.70	0.39	13.09	0.53	10.10	0.69	7.30	0.96
G-13-NC-52.1-2	5.13	14.10	0.36	10.05	0.51	15.91	0.32	17.70	0.29	13.09	0.39	10.10	0.51	7.30	0.70
G-13-NC-52.1-3	6.42	14.10	0.46	10.05	0.64	15.91	0.40	17.70	0.36	13.09	0.49	10.10	0.64	7.30	0.88
G-13-NC-52.1-1*	10.78	14.10	0.76	10.05	1.07	15.91	0.68	17.70	0.61	13.09	0.82	10.10	1.07	7.30	1.48
G-13-NC-52.1-2*	10.19	14.10	0.72	10.05	1.01	15.91	0.64	17.70	0.58	13.09	0.78	10.10	1.01	7.30	1.40
G-13-NC-52.1-3*	9.87	14.10	0.70	10.05	0.98	15.91	0.62	17.70	0.56	13.09	0.75	10.10	0.98	7.30	1.35
G-13-65%-21.5-1	10.49	9.06	1.16	6.45	1.63	10.22	1.03	11.37	0.92	13.09	0.80	7.75	1.35	4.69	2.24
G-13-65%-21.5-2	10.80	9.06	1.19	6.45	1.67	10.22	1.06	11.37	0.95	13.09	0.83	7.75	1.39	4.69	2.30
G-13-65%-21.5-3	10.78	9.06	1.19	6.45	1.67	10.22	1.05	11.37	0.95	13.09	0.82	7.75	1.39	4.69	2.30
B-12-50%-45.4-1	13.03	13.26	0.98	10.16	1.28	14.85	0.88	17.11	0.76	13.09	1.00	9.70	1.34	7.38	1.76
B-12-50%-45.4-2	10.91	13.26	0.82	10.16	1.07	14.85	0.73	17.11	0.64	13.09	0.83	9.70	1.13	7.38	1.48
B-12-50%-45.4-3	11.31	13.26	0.85	10.16	1.11	14.85	0.76	17.11	0.66	13.09	0.86	9.70	1.17	7.38	1.53

TV = Test value of bond strength, PV = Predicted value of bond strength, COV = The ratio of bond strength of test value and predicted value

Table 7 The comparison of the test values and predicted values of bond strength using the formulas of FRP reinforced SCC (Eqs. 9 and 11)

Specimen[a]	TV (MPa)	(9)		(11)	
		PV (MPa)	COV	PV (MPa)	COV
G-13-50%-45.4-1	10.81	19.37	0.56	10.84	1.00
G-13-50%-45.4-2	11.10	19.37	0.57	10.84	1.02
G-13-50%-45.4-1*	13.10	19.37	0.68	10.84	1.21
G-13-50%-45.4-2*	10.89	19.37	0.56	10.84	1.00
G-13-50%-45.4-3*	11.39	19.37	0.59	10.84	1.05
G-19-50%-45.4-1	2.71	13.93	0.19	3.84	0.71
G-19-50%-45.4-2	4.44	13.93	0.32	3.84	1.16
G-19-50%-45.4-3	3.53	13.93	0.25	3.84	0.92
G-13-65%-21.5-1	10.49	13.33	0.79	10.73	0.98
G-13-65%-21.5-2	10.80	13.33	0.81	10.73	1.01
G-13-65%-21.5-3	10.78	13.33	0.81	10.73	1.00
B-12-50%-45.4-1	13.03	20.81	0.63	12.68	1.03
B-12-50%-45.4-2	10.91	20.81	0.52	12.68	0.86
B-12-50%-45.4-3	11.31	20.81	0.54	12.68	0.89

Table 8 Parameter calibration of the Malvar, mBPE and CMR models

Specimen	τ_b (MPa)	S_b (mm)	F	G	α	p	S_r	β
G-13-50%-45.4-1*	13.100	7.419	11.126	−2.132	0.170	0.211	3.035	0.244
G-13-50%-45.4-2*	10.893	9.037	9.935	−2.548	0.109	0.369	2.969	0.165
G-13-50%-45.4-3*	11.390	7.047	22.751	−6.368	0.150	0.186	1.244	0.303
Mean value	11.794	7.834	14.604	−3.683	0.143	0.255	2.416	0.237
G-13-NC-52.1-1*	10.779	6.537	5.435	−0.211	0.246	0.243	1.098	0.712
G-13-NC-52.1-2*	10.189	8.439	4.612	−0.468	0.209	0.366	4.121	0.280
G-13-NC-52.1-3*	9.865	8.522	3.086	0.080	0.226	0.392	2.617	0.448
Mean value	10.278	7.832	4.378	−0.200	0.227	0.334	2.612	0.480

$$l_{ab} = f_{max} A_r / \tau_{max} \pi d = \frac{f_{max} d}{4\tau_{max}} \quad (13)$$

The bond strength in Eq. (11) is substituted into Eq. (13) to obtain the minimum development length of the FRP reinforce HVFA-SCC component, and it can be expressed as follows:

$$l_{ab} = \frac{f_{max} d}{4\sqrt{f_c}\left(-9.3508 + 0.4778\frac{c}{d} + 0.0108 \times SF\right)} \quad (14)$$

To ensure a positive bond strength in Eq. (11) and avoid negative development length in Eq. (14), the ratio of the thickness of the concrete protective layer to the diameter of FRP bar should be set within a reasonable range, which can be obtained as follows:

$$\frac{c}{d} > 19.5705 - 0.0226SF; \quad 550 \le SF \le 850 \quad (15)$$

4.2 Analytical modelling of bond-slip curve

Currently, some available analytical models [42–44] for the bond-slip relationship of FRP reinforced concrete components have been proposed by using curve-fitting of the test data to determine the parameters, which aim to identify bond-slip law. Those models are generally developed to evaluate the bond behaviour and failure mechanism in the bond-slip tests. Additionally, a suitable bond-slip model is beneficial to develop accurate numerical modelling and simulation. However, a suitable bond-slip law has not been proposed for FRP reinforced HVFA-SCC structures due to many factors that have strong effects on bond performance, including the different behaviours and failure mechanisms involved in various concrete matrix materials and reinforcing materials. In this study, three commonly used theoretical models, including the Malvar model, the modified BPE (mBPE) model, and the CMR model were used to predict the bond-slip behaviour of FRP reinforced HVFA-SCC.

The Malvar model [42] is a polynomial function which was proposed to predict the bond-slip performance, as shown in Eq. (16):

$$\tau = \tau_b \frac{F\left(\frac{s}{s_b}\right) + (G-1)\left(\frac{s}{s_b}\right)^2}{1 + (F-2)\left(\frac{s}{s_b}\right) + G\left(\frac{s}{s_b}\right)^2} \tag{16}$$

where τ and s represent the bond stress and the slip, τ_b and τ_b s_b are bond strength and its corresponding slip obtained from test results; F and G are parameters to be determined by fitting test data. It is noted that the using Malvar model results in a low prediction accuracy for the ascending segment due to the single expression. Also, the effect of bar diameter on the bond strength is ignored in the Malvar model.

The modified BPE (mBPE) model was described by Cosenza et al. [45] and is presented in Eq. (17), as follows:

$$\frac{\tau}{\tau_b} = \left(\frac{s}{s_b}\right)^{\alpha} \quad \text{for} \quad 0 \le s \le s_b \tag{17a}$$

$$\tau_{max} = 1 - p\left(\frac{s}{s_b}\right) \quad \text{for} \quad s_b < s \le s_3 \tag{17b}$$

$$\tau = \tau_3 \quad \text{for} \quad s_b < s \le s_3 \tag{17c}$$

where α and p are the curve-fitting parameters based on test data. The effects of type and diameter of FRP bars are not considered in this model.

The CMR model suggested by Cosenza et al. [42] can be expressed as follows:

$$\frac{\tau}{\tau_b} = \left(1 - e^{-s/s_r}\right)^{\beta} \tag{18}$$

where s_r and β are the parameters that can be obtained by fitting test data. The slope of the initial stage of the CMR model is infinite, which better matches the physical meaning of chemical adhesion. However, the descending branches of the bond-slip curve are not represented in the CMR model.

Equations 16–18 are calibrated based on the test results of FRP reinforced HVFA-SCC test specimens in this study. Considering that the bond behaviour of the reinforcing bar with a low spiral height is easily affected by interfacial pores of concrete materials, those specimens of GFRP with a spiral height of 0.51 mm reinforced concrete are selected to calibrate the parameters of the analytical models. These parameters are determined by using the least square method are listed in Table 8 and the predicted bond-slip curves are shown in Fig. 6. It can be observed that the initial stiffness of the bond-slip curves is underestimated, and the tested results of the ascending branches cannot be accurately evaluated by the Malvar model. However, the test results of bond-slip curves are consistent with the predicted results by using the mBPE model. It is worth mentioning that the third equation (Eq. (17c)) of the mBPE model should be used based on the characteristics of the bond-slip curves of FRP reinforced concrete obtained from the experiment. If a stable residual segment, i.e. the phenomenon that the bond stress remains constant as the unloaded end slip continues to increase, was not found in the test results, the third equation (Eq. (17c)) of the mBPE model can be removed to predict the bond-slip behaviour.

In general, the bond-slip behaviour after peak bond stress cannot be predicted by using CMR model. Compared with the Malvar model, the mBPE model composed of piecewise expressions is more accurate in predicting the bond-slip behaviour of FRP reinforced HVFA-SCC and FRP reinforced NC. Furthermore, suggested values of the parameters of the mBPE model are determined and calibrated for FRP

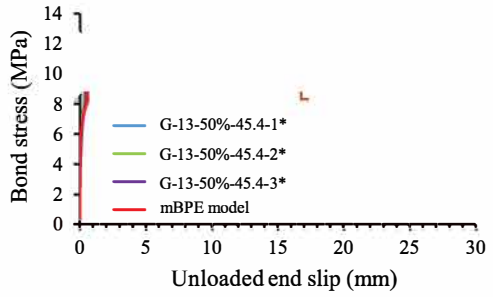

(a) Comparison of the bond-slip curves between the test results (specimen coded G-13-50%-45.4*) and the predicted results (mBPE model)

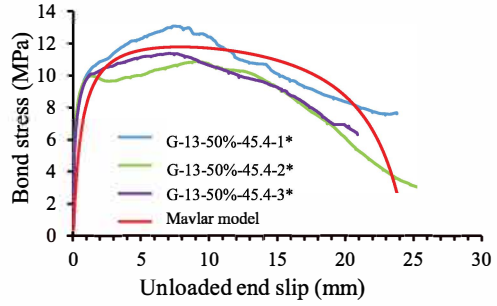

(b) Comparison of the bond-slip curves between the test results (specimen coded G-13-50%-45.4*) and the predicted results (Mavlar model)

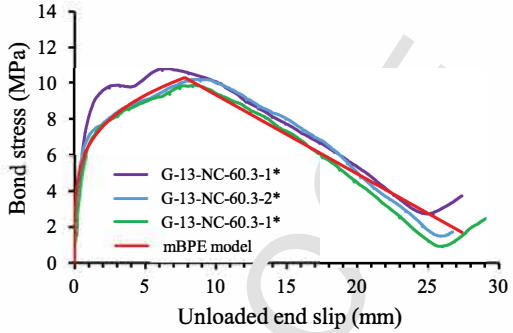

(c) Comparison of the bond-slip curves between the test results (specimen coded G-13-NC-60.3*) and the predicted results (mBPE model)

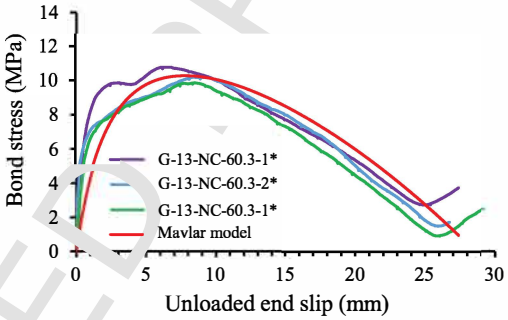

(d) Comparison of the bond-slip curves between the test results (specimen coded G-13-NC-60.3*) and the predicted results (Mavlar model)

Fig. 6 Comparison of the bond-slip relationship test results and the predicted results by the Malvar model and the mBPE model

reinforced HVFA-SCC specimens based on the obtained experimental data, which is of great significance for the numerical and theoretical studies of FRP reinforced HVFA-SCC members considering the bond-slip constitutive model in the future research.

5 Conclusions

In this paper, the bond-slip behaviour of FRP reinforced HVFA-SCC has been investigated through a series of pull-out tests. The influence of parameters, such as the type of reinforcing bars, the geometry of the surface of GFRP bars, the bar diameters and the concrete material type, on the bond-slip behaviour is discussed. Based on the test and analysis results, the following conclusions can be drawn:

1. The average bond strength of steel bar reinforced HVFA-SCC is about two times higher than that of GFRP bar and BFRP bar reinforced HVFA-SCC. The use of large diameter FRR bars results in a significant reduction in bond strength. The bond strength can be improved using HVFA-SCC instead of NC reinforced with GFRP bars, especially in GFRP with a lower spiral height. The average bond strength of HVFA-SCC specimens is improved slightly, while the average bond strength of NC specimens is increased by about 80% when the spiral height of GFRP bars is from 0.21 to 0.51 mm.
2. The bond failure of the GFRP and BFRP reinforced test specimens depends on friction and chemical adhesion. While the bonding failure of the steel reinforced test specimens is controlled by mechanical interlocking. The surface damage on the GFRP bar of the HVFA-SCC series is more pronounced than in the NC series. This indicates that stronger chemical adhesion is presented in FRP reinforced HVFA-SCC. In addition, the surface damage of the GFRP bar with a spiral height of 0.51 mm is more severe than that of the 0.21 mm.
3. The bond behaviours, including initial bond stiffness, bond strength and bonding degradation, are significantly affected by the type of reinforcement. Rapid degradation after peak bond stress occurs in GFRP reinforced HVFA-SCC with 65%

fly ash instead of cement, which could be related to the compressive strength of concrete materials.
4. The prediction formula of the bond strength of FRP reinforced HVFA-SCC considering slump-flow is proposed, and the formula for the minimum development length of the HVFA-SCC component reinforced with FRP bars is established.
5. The parameters of those analytical models for FRP reinforced NC and HVFA-SCC specimens are calibrated based on the experimental data. The mBPE model based on calibration parameters the can accurately predict the bond-slip behaviour of FRP reinforced HVFA-SCC and NC.

Acknowledgements This work was partially supported by the Natural Science Foundation of China (51678149), the Key Research Project by Department of Education of Guangdong Province, China (2018KZDXM068), the Key Research Project of Social Science and Technology of Dongguan City, China (20185071401603) and the Innovation Group Supported by Department of Education of Guangdong Province (2019KCXTD013). The authors are sincerely grateful for these partial financial supports.

Author contributions Yu Zheng and Haotian Li conceived and designed the experiments; Lingzhu Zhou, Nuan Zhou and Haotian Li performed the experiments; Haotian Li, Nuan Zhou, Lingzhu Zhou, Yu Zheng and Yingwu Zhou analyzed the data; Lingzhu Zhou wrote the paper; Yu Zheng and Henxin Zhang revised the paper.

Compliance with ethical standards

Conflict of interest The authors declare no conflicts of interest.

References

1. Chernin L, Val DV (2011) Prediction of corrosion-induced cover cracking in reinforced concrete structures. Constr Build Mater 25(4):1854–1869
2. McLellan BC, Williams RP, Lay J, Riessen A et al (2011) Costs and carbon emissions for geopolymer pastes in comparison to ordinary Portland cement. J Clean Prod 19(9)
3. Lingzhu Z, Yu Z, Susan T (2018) Finite-element investigation of the structural behavior of basalt fiber reinforced polymer (BFRP)-reinforced self-compacting concrete (SCC) decks slabs in thompson bridge. Polymers 10(6):678
4. García-Taengua E, Sonebi M, Crossett P et al (2016) Performance of sustainable SCC mixes with mineral additions for use in precast concrete industry. J Sustain Cem Based Mater 5(3):157–175
5. Sonebi M, Nanukuttan S (2009) Transport properties of self-consolidating concrete. ACI Mater J 106(2):161–166
6. Alghazali HH, Myers JJ (2017) Shear behavior of full-scale high volume fly ash-self consolidating concrete (HVFA-SCC) beams. Constr Build Mater 157:161–171
7. Yu Z, Lingzhu Z, Lipeng X, Yuanbin L, Taylor SE (2018) Investigation of the behaviour of scc bridge deck slabs reinforced with bfrp bars under concentrated loads. Eng Struct 171:500–515
8. Zheng Y, Zhou L, Taylor SE, Ma H (2019) Serviceability of one-way high-volume fly ash-self-compacting concrete slabs reinforced with basalt FRP bars. Constr Build Mater 217:108–127
9. Zheng Y, Zhou L, Xia L, Luo Y, Taylor SE (2018) Investigation of the behaviour of SCC bridge deck slabs reinforced with BFRP bars under concentrated loads. Eng Struct 171:500–515
10. Benmokrane B, Tighiouart B, Chaallal O (1996) Bond strength and load distribution of composite gfrp reinforcing bars in concrete. ACI Mater J 93(3):246–253
11. Malvar LJ (1995) Tensile and bond properties of gfrp reinforcing bars. ACI Mater J 92(3):276–285
12. Okelo R, Yuan RL (2005) Bond strength of fiber reinforced polymer rebars in normal strength concrete. J Compos Constr 9(3):203–213
13. Achillides Z, Pilakoutas K (2004) Bond behavior of fiber reinforced polymer bars under direct pullout conditions. J Compos Constr 8(2):173–181
14. Yu Z, Dongdong C, Lingzhu Z, Linsheng H, Hongwei M, Gangbing S (2018) Evaluation of the effect of fly ash on hydration characterization in self-compacting concrete (SCC) at very early ages using piezoceramic transducers. Sensors 18(8):2489
15. Zhou L, Zheng Y, Yu Y, Song G, Huo L, Guo Y (2020) Experimental study of mechanical and fresh properties of HVFA-SCC with and without pp fibers. Constr Build Mater
16. Ojarestaghi SSM, Ajarostaghi SSM, Bhojaraju C (2020) A critical review of the effect of concrete composition on rebar–concrete interface (RCI) bond strength: a case study of nanoparticles. SN Appl Sci 2(5):1–23
17. Chen F, Li CQ, Baji H, Ma B (2019) Effect of design parameters on microstructure of steel-concrete interface in reinforced concrete. Cem Concr Res 119:1–10
18. Emadaldin M, Golafshani A, Rahai M (2014) Bond behavior of steel and GFRP bars in self-compacting concrete. Constr Build Mater
19. Sfikas IP, Trezos KG (2013) Effect of composition variations on bond properties of self-compacting concrete specimens. Constr Build Mater 41:252–262
20. Arezoumandi M, Wolfe MH, Volz JS (2013) A comparative study of the bond strength of reinforcing steel in high-volume fly ash concrete and conventional concrete. Constr Build Mater 40:919–924
21. Martí-Vargas JR, Serna P, Navarro-Gregori J, Bonet JL (2012) Effects of concrete composition on transmission length of prestressing strands. Constr Build Mater 27(1):350–356
22. Zhou L, Zheng Y, Li H, Song G (2020) Identification of bond behavior between FRP/steel bars and self-compacting concrete using piezoceramic transducers based on wavelet energy analysis. Arch Civ Mech Eng. https://doi.org/10.1007/s43452-020-00041-1

23. Arias JPM, Vazquez A, Escobar MM (2012) Use of sand coating to improve bonding between gfrp bars and concrete. J Compos Mater 46(18):2271–2278
24. ACI Committee (2012) ACI 440.3 R-2012 guide test methods for fiber-reinforced polymer (FRP) composites.American Concrete Institute, Farmingon Hills
25. Kuo WT, Liu MY, Juang CU (2019) Bonding behavior of repair material using fly-ash/ground granulated blast furnace slag-based geopolymer. Materials 12(10):1697
26. Wang YL, Wang WD, Guan XM (2011) Physical filling effects of limestone powders with different particle size. Adv Mater Res 163–167:1419–1424
27. Baena M, Torres L, Turon A, Barris C (2009) Experimental study of bond behaviour between concrete and frp bars using a pull-out test. Compos A Appl Sci Manuf 40b(8):784–797
28. Danying G, Benmokrane B (2001) Influential factors of bond properties between fiber reinforced polymer (frp) rebars and concrete. Ind Constr
29. Bazant ZP, Sener S (1988) Size effect in pullout tests. ACI Mater J 85(5):347–351
30. Wu C, Chen G (2015) Unified model of local bond between deformed steel rebar and concrete: indentation analogy theory and validation. J Eng Mech 141(10):04015038
31. Darwin D, Graham EK (1993) Effect of deformation height and spacing on bond strength of reinforcing bars. ACI Mater J 90(6):646–657
32. Gu X, Yu B, Wu M (2016) Experimental study of the bond performance and mechanical response of gfrp reinforced concrete. Constr Build Mater 114:407–415
33. Rukzon S, Chindaprasirt P (2013) Chloride penetration and corrosion resistance of ground fly ash blende. Int J Mater Res 102(3):335–339
34. CEB-FIP, Model Code 1990 (1990) Comité Euro-International de Béton.Thomas Telford Services Ltd., London
35. ACI Committee (2006) ACI 440.1R-06 Guide for the design and construction of concrete reinforced with FRP bars. American Concrete Institute, Farmingon Hills
36. ACI Committee (2003) ACI 440.1R-03 Guide for the design and construction of concrete reinforced with FRP bars.American Concrete Institute, Farmingon Hills
37. CEB-FIP (2007) FRP reinforcement in RC structures. Fib bulletin 40. International Federation for Structural Concrete (FIB)
38. Choi DU, Chun SC, Ha SS (2012) Bond strength of glass fibre-reinforced polymer bars in unconfined concrete. Eng Struct 34:303–313
39. He Z, Tian GW (2011) Probabilistic evaluation of the design development length of a gfrp rod pull-out from concrete. Eng Struct 33(10):2943–2952
40. Lee JY, Kim TY, Kim T, Yi CK, Park JS, You YC et al (2008) Interfacial bond strength of glass fiber reinforced polymer bars in high-strength concrete. Compos B Eng 39B(2):258–270
41. Mousavi S, Dehestani M, Mousavi S (2016) Bond strength and development length of glass fiber-reinforced polymer bar in unconfined self-consolidating concrete. J Reinf Plast Compos 35(11):924–941
42. Cosenza E, Manfredi G, Realfonzo R (1995) Analytical modelling of bond between FRP reinforcing bars and concrete. Non-metallic (FRP) reinforcement for concrete structures. In: Proceedings of the second international RILEM symposium (FRPRCS-2)
43. Antonietta Aiello M, Leone M, Pecce M (2007) Bond performances of frp rebars-reinforced concrete. J Mater Civ Eng 19(3):205–213
44. Rossetti VA, Galeota D, Giammatteo MM (1995) Local bond stress-slip relationships of glass fibre reinforced plastic bars embedded in concrete. Mater Struct 28(6):340–344
45. Eligehausen R, Popov EP, Bertero VV (2016) Local bond stress–slip relationships of deformed bars under generalized excitations